Supporting Information

Unraveling the Morphology–Function Relationships of Polyamide Membranes Using Quantitative Electron Tomography

Xiaohui Song,[†,°] John W. Smith,[†,°] Juyeong Kim,[†,‡,▽] Nestor J. Zaluzec,[⊥] Wenxiang Chen,[†,‡] Hyosung An,[†,‡] Jordan M. Dennison,[§] David G. Cahill,[†,‡] Matthew A. Kulzick,[#] and Qian Chen[,†,‡,§,∥]*

[†]Department of Materials Science and Engineering, [‡]Materials Research Laboratory, [§]Department of Chemistry, and [∥]Beckman Institute for Advanced Science and Technology, University of Illinois at Urbana-Champaign, Urbana, Illinois 61801, United States

[⊥]Photon Sciences Division, Argonne National Laboratory, Argonne, Illinois 60439, United States

[#]BP Corporate Research Center, Naperville, Illinois 60563, United States

°Equal contribution

[▽]Current address: Department of Chemistry and Research Institute of Natural Sciences, Gyeongsang National University, Jinju 52828, Republic of Korea

*To whom correspondence should be addressed. Email: qchen20@illinois.edu

Supplementary Methods

Chemicals

Cadmium chloride hydrate (99.998%, $CdCl_2 \cdot xH_2O$, x ≈ 2.5, Alfa Aesar), ethanolamine (>98%, $NH_2CH_2CH_2OH$, Sigma-Aldrich), *m*-phenylenediamine (MPD, 99%, C_6H_4-1,3-$(NH_2)_2$, Sigma-Aldrich), 1,3,5-benzenetricarbonyl trichloride (a.k.a. trimesoyl chloride, TMC, 98%, $C_6H_3(COCl)_3$, Sigma-Aldrich), molecular sieves (3Å, 1–2 mm beads, Alfa Aesar), hydrochloric acid (36.5–38.0%, HCl, 2.5 L, Macron), zinc nitrate hexahydrate (98%, $Zn(NO_3)_2 \cdot 6H_2O$, Sigma-Aldrich), lead nitrate (>95%, $Pb(NO_3)_2$, Fisher Scientific), polysulfone (PS35, Sepro Corporation), and methanol (99.9%, CH_4O, Fisher Chemical) were used without further purification. Hexanes (99.9%, C_6H_{14}, Fisher Chemical) were stored with approximately 250 mL molecular sieves in a 1 L glass jar for 1 day before use. All glassware was cleaned in a base bath (saturated potassium hydroxide in isopropyl alcohol) followed by an acid bath (1 M hydrochloric acid), fully rinsed with water, and dried under nitrogen gas immediately before use. Water used in this work was purified by a Milli-Q Advantage A10 system (18.2 MΩ·cm at 25 °C). Note that cadmium chloride hydrate, MPD, and TMC were carefully stored in a desiccator to prevent exposure to moisture. It was found that this precaution was critical for reproducible membrane synthesis.

Synthesis of a free-floating polyamide (PA) film

PA films were synthesized with adaptations to a literature method.[1] A polysulfone (PSf) substrate (~8 cm × ~5 cm) was fixed on a glass filter funnel (5.7 cm outer diameter, 3.8 cm inner diameter) connected to a filtering flask, in turn connected to a vacuum pump (KNF, UN726.3 FTP). The PSf was stored in water for at least 12 h to hydrate its pores. Methanol (~50 mL) was filtered through the PSf, followed by water (~50 mL).

Cadmium hydroxide nanowires were synthesized by sequential addition of aqueous solutions of $CdCl_2 \cdot xH_2O$ (50 mL, 4 mM) and ethanolamine (50 mL, 2 mM) to a 250 mL Erlenmeyer flask stirring with a magnetic stir bar at 500 rpm at room temperature. The solution turned cloudy and was stirred for 15 min. The solution of cadmium hydroxide nanowires was poured onto the filter, and then filtered across the PSf substrate with a vacuum pump. The filtration speed was controlled using a valve control attached to the vacuum pump, such that the 100 mL total reaction volume was filtered over the course of 50 min (i.e., ~2 mL min^{-1}).

Immediately after the nanowire solution was filtered across the PSf, an aqueous solution of MPD (25 mL, 2 wt%) was gently transferred onto the PSf substrate using a 10 mL micropipette. It took approximately 20 min for the MPD solution to flow into the PSf substrate completely, whereupon the vacuum pump was turned off. Note that the addition of MPD needs to be gentle, by controlling the pipetting speed and angle, so as not to disturb the settled cadmium hydroxide wires. To initiate interfacial polymerization, TMC in hexanes (25 mL, 0.1 wt%) was added to the PSf containing MPD. The TMC solution was left on the PSf for 1 min. Then the reaction was terminated by gently removing the TMC solution with a 10 mL micropipette. Pure hexanes (10 mL) were added onto the PSf and removed immediately to rinse away any residual TMC. The PSf was rinsed with hexanes two more times.

PSf with the polymerized PA film on top was placed in a Petri dish (10.0 cm in diameter) with water for one additional rinsing step and then transferred to another Petri dish containing 10 mM HCl. The PA film was released from the PSf after about 30 min (etching times varied to some extent) due to the etching of the cadmium hydroxide nanowire sublayer by HCl. The PA film was kept soaking in the same HCl solution overnight to completely remove any remaining cadmium hydroxide nanowires.

PA film characterization

A JEOL 2100 Cryo or JEOL 2010 LaB_6 TEM operating at 200 kV was used for imaging PA film morphology (Figure 1d). The grids used were 400-mesh copper grids with a uniform carbon film (Electron Microscopy Sciences, CF400-Cu).

The roughness of PA films was measured using tapping-mode atomic force microscopy (AFM, Asylum Research Cypher). A free-floating PA film in water was gently scooped onto a Si wafer (0.5 cm × 0.5 cm). The Si wafer had been washed three times in isopropanol, three times in water, and another three times in ethanol before being dried with N_2 gas. The sample was further dried in desiccator at room temperature for 6 hours before being used for AFM characterization (Figure S1).

Transmission electron microscopy (TEM) tomography

A series of tilt images of a PA film were acquired using a JEOL 2100 Cryo TEM. A low electron beam dose rate (7.4 $e^- Å^{-2} s^{-1}$) was applied using spot size 3. Each image was collected with a 3 s exposure time, resulting in a dose per image of 22.2 $e^- Å^{-2}$. The tilt angle ranged from −60° to 60° in 2° increments. After manually setting the eucentric height at each tilt angle, the image was defocused by −3072 nm to improve contrast, and the same defocus was applied to all the images at different tilt angles. The open-source software IMOD 4.9.3 (University of Colorado, http://bio3d.colorado.edu/) was used to align and assemble TEM images.[2] Since no fiducial markers were used, a patch tracking mode was applied, and the tomogram was generated using the default weighted back-projection algorithm available in IMOD. Segmentation and three-dimensional (3D) morphology analysis were performed in ImageJ/FIJI[3] and Amira 6.4[4] (FEI).

Image processing and 3D morphometry

The reconstructed 3D PA film was imported into Amira, which was used for preliminary image processing, segmentation, and 3D morphology analysis. First, regions containing a single crumple were selected by cropping. Then a 3D Gaussian filter with a standard deviation of 2 pixels in all directions and a kernel size of 9 pixels was applied. Contrast and brightness were then adjusted using the "Brightness-Contrast" command under "Grayscale transforms" without changing any settings (Figure S2a). A grayscale threshold was then set on a per-crumple basis in order to generate an approximately segmentated volume (Figure S2b), which was then corrected using a combination of the Dilate/Erode commands and manual adjustment to fill in holes or remove regions not corresponding to the crumple. The 3D volume, surface area, and void volume of each crumple given in Table S1 were measured by performing the "Individual Measures" command on the thresholded label file and selecting the appropriate values to be calculated under "Measure". The remaining values in Table S1 were determined from these measurements based on their definition.

Segmented crumples were converted to a network of triangular meshes with Amira's "Generate Surface" function using a mesh size of 2.6 nm for all crumples. This mesh was smoothed using the "Smooth Surface" function with the number of iterations set to 4 and $\lambda = 0.7$ (Figure S4). Principal curvature values $\kappa_1$and κ_2 at each triangle were calculated with the Curvature option set to "BothCurvatures." Gaussian (G) and mean (H) curvatures were determined according to their definition (i.e., $G = \kappa_1\kappa_2$ and $H = (\kappa_1 + \kappa_2)/2$). Curvature elements at each triangle were determined with an "Arithmetic" expression of the form:

$$(\kappa_1 > 0 \;\&\&\; \kappa_2 > i) + 2(\kappa_1 > 0 \;\&\&\; \kappa_2 < i \;\&\&\; \kappa_2 > j)$$

$$+3(\kappa_1 > 0 \;\&\&\; \kappa_2 < j) + 4(\kappa_1 < 0 \;\&\&\; \kappa_2 < j)$$

where "&&" is the Boolean "and". In this way, the expression returns 1 if the triangle is a "tip" element, 2 if it is a "tube" element, 3 if it is a "saddle" element, and 4 if it is a "valley" element. Note that Amira stores $\kappa_1$and κ_2 as a single "complex" number, so they can be accessed by the Arithmetic function as "Ar" and "Ai," respectively in the "BothCurvatures" output. Thresholds i and j were chosen because the second principal curvature (and therefore G) at "tube" elements is never perfectly zero (i.e., the film is never perfectly flat). Values of i and j were defined on a per-crumple basis, by examining the distribution of κ_2 values for each crumple (Figure S7). Each κ_2 distribution has a sharp peak around zero curvature, and values on either side of the base of this peak were chosen as i and j accordingly. Threshold values for each crumple are given in Table S4.

Local thicknesses of crumples and void spaces were calculated by exporting segmented crumples as stacks of binary images and using the Local Thickness plugin[5] in FIJI/ImageJ. The local thickness at a given point is defined as the size of the largest sphere that contains the point and remains within the bounds of the structure. The Local Thickness algorithm consists of three steps. First, each point in a binarized volume is assigned a grayscale value according to how far it is from the edge of the shape. Points deep within the volume are brighter, and points near surfaces are darker. The result is that local maxima appear approximately half-way between two boundaries of the volume. These local maxima form "ridges" which, effectively, trace the center positions of the largest spheres that can fit in those regions. The algorithm, then, continues by first tracing these ridges (the centers of the largest spheres) and then using the grayscale values along them (which are proportional to the size of those spheres) to determine the local thickness at each nearby point.

In skeletonization, a 3D volume is iteratively thinned until lines only a single voxel thick remain. To perform skeletonization, segmented volumes were thinned with the "Auto Skeleton" function

in Amira using default settings. Node coordinates and connectivities, as well as branch lengths were calculated from the "Spatial Graph" output generated from each skeletonization procedure.

Ion adsorption and scanning TEM energy dispersive X-ray spectroscopy (STEM-EDXS)

A small piece of PA film (<3 mm in diameter) was transferred to a small Petri dish (6 cm in diameter) containing 5 mL water. The film was left floating on the water surface for 24 h to draw off residual HCl and any other chemicals from the synthesis and nanowire etching. Then, the water was removed using a micropipette and an aqueous solution of metal salts (5 mL of 540 mM $Pb(NO_3)_2$ and 5 mL 540 mM $Zn(NO_3)_2$) was added to the Petri dish. The PA film was incubated in the mixed metal salt solution for 24 h to allow the metal ions to adsorb to the PA film. Then the metal solution was removed using a micropipette (until no liquid was visible in the Petri dish) and 5 mL of fresh water was added to the Petri dish to rinse off excess salt. The film was quickly scooped onto a TEM grid (Quantifoil R 1/4 Holey Carbon, 300 Mesh, Gold, Electron Microscopy Sciences). The grid was dried for 3–4 h at room temperature before imaging. The use of a holey carbon film prevented the metal solution getting trapped between the carbon film and the PA film, while a gold grid mesh was chosen to prevent overlap between the X-ray emission spectra of zinc (K_α = 8.63) and copper found in conventional TEM grids (K_α = 8.04).

EDXS was performed on an FEI Talos F200X TEM/STEM with a field emission gun and a SuperX energy-dispersive spectrometer and an FEI Tecnai F20ST TEM/STEM in the Center for Nanoscale Materials at Argonne National Laboratory. An accelerating voltage of 200 kV was used. Raw elemental maps were background-corrected and denoised with a 3-pixel average. Colocalizations were calculated in ImageJ.

Figures S1–S7

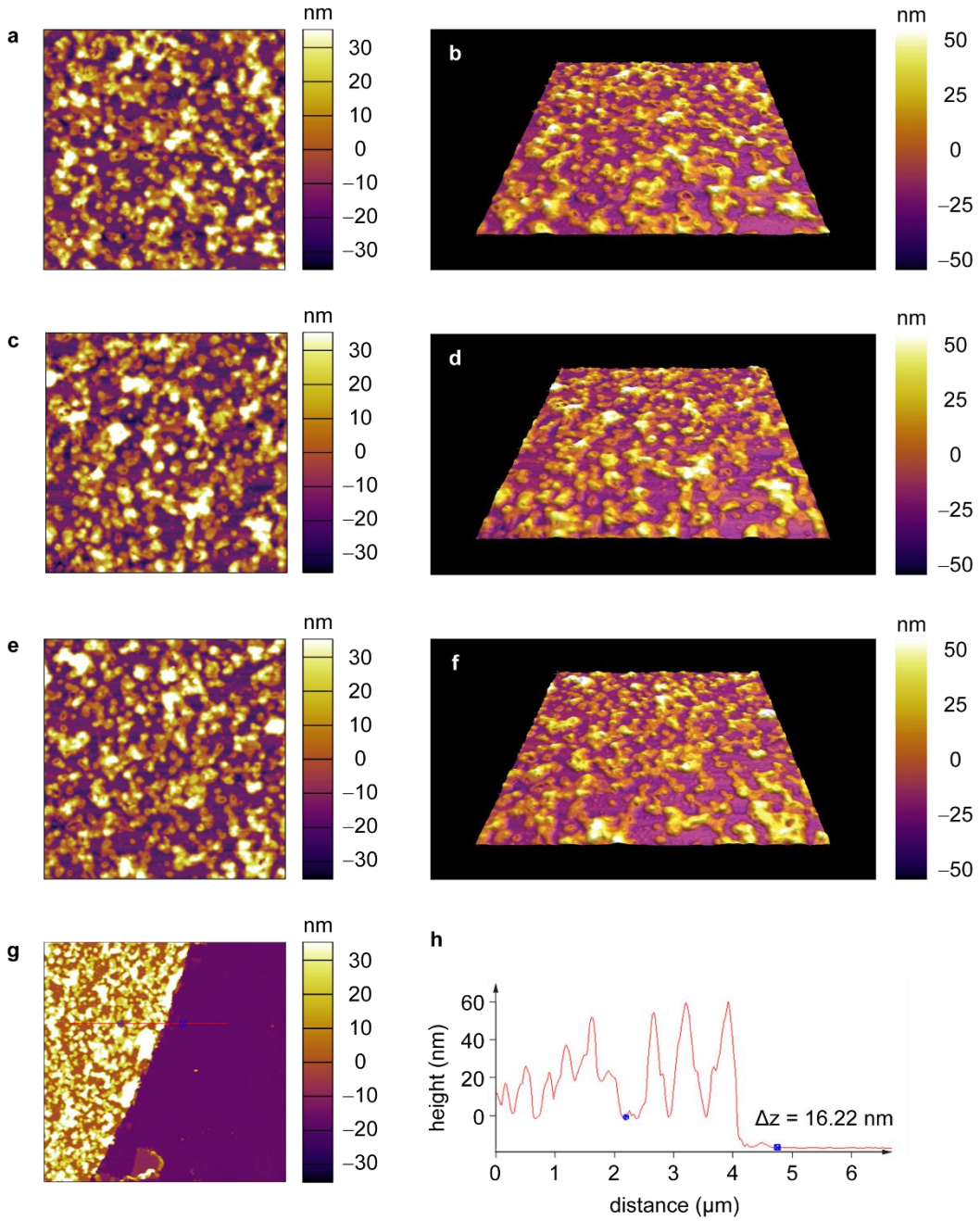

Figure S1. AFM scans of the PA films synthesized for imaging and analysis in Figures 1–4: a–b) area 1 with root-mean-square (RMS) roughness 18.4 nm. c–d) area 2 with RMS roughness 17.9 nm. e–f) area 3 with RMS roughness 17.6 nm. g) AFM scan across the film edge onto the silicon substrate. h) *z* trace along the line marked in red in (g). The height difference Δ*z* between a region in the flat part of the membrane (left blue dot) and the substrate (right blue dot) is 16.22 nm. Scans in a–f are 5 μm by 5 μm. The scan in g is 10 μm by 10 μm. AFM procedures are described in the Supplementary Methods.

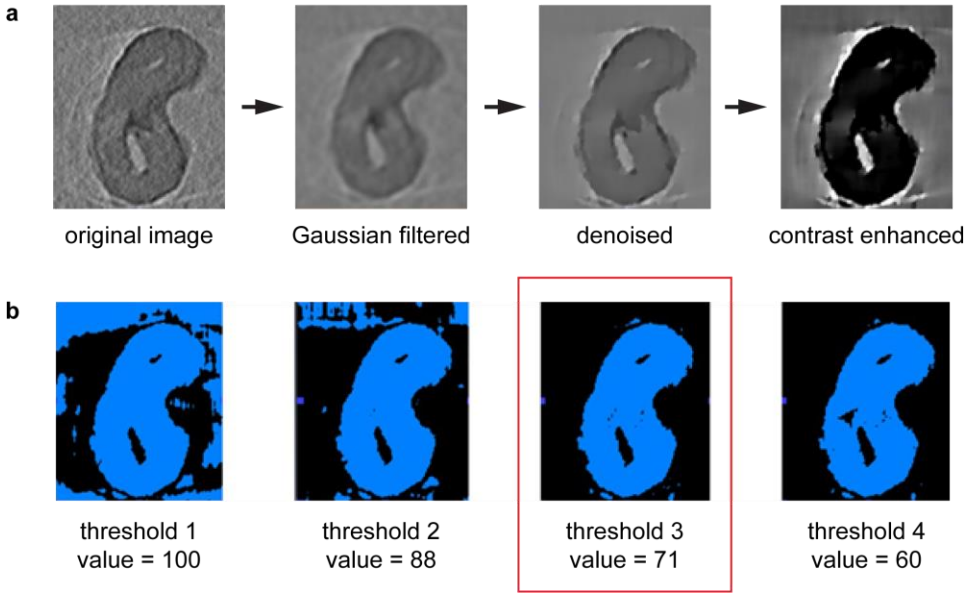

Figure S2. Image processing and segmentation workflow. a) After a volume containing an individual crumple was cropped from the full reconstruction, the image processing pipeline consisted of Gaussian filtering (kernel size 9), denoising, and contrast enhancement using built-in Amira functions. b) Contrast-enhanced images were thresholded (in this case, because the crumple is dark, voxels with a grayscale value above some threshold become background and all others become foreground). A variety of thresholds were tested for each crumple, and the best (in this case, the one in the red box) was selected for manual correction of remaining small holes and bumps. Further image processing details are described in the Supplementary methods.

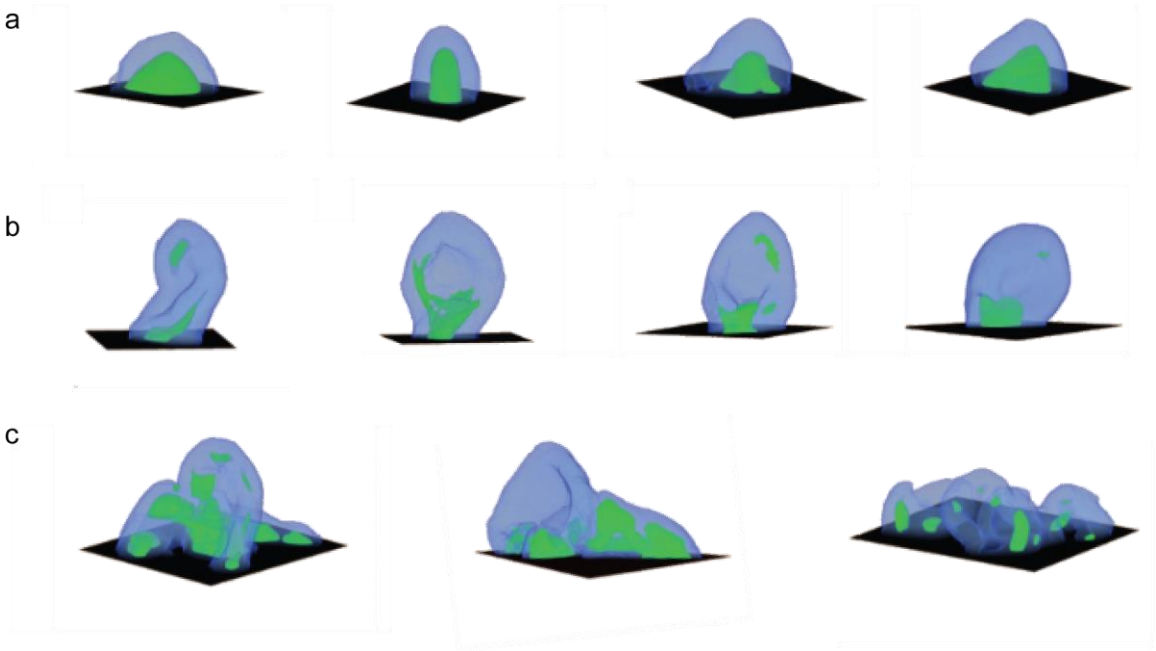

Figure S3. 3D images of different crumples, with the membrane portions rendered in blue and the void spaces enveloped by the membrane rendered in green. a) domes 1–4, b) dimples 1–4, and c) clusters 1–3. Size parameters for the film and void spaces are summarized in Table S1.

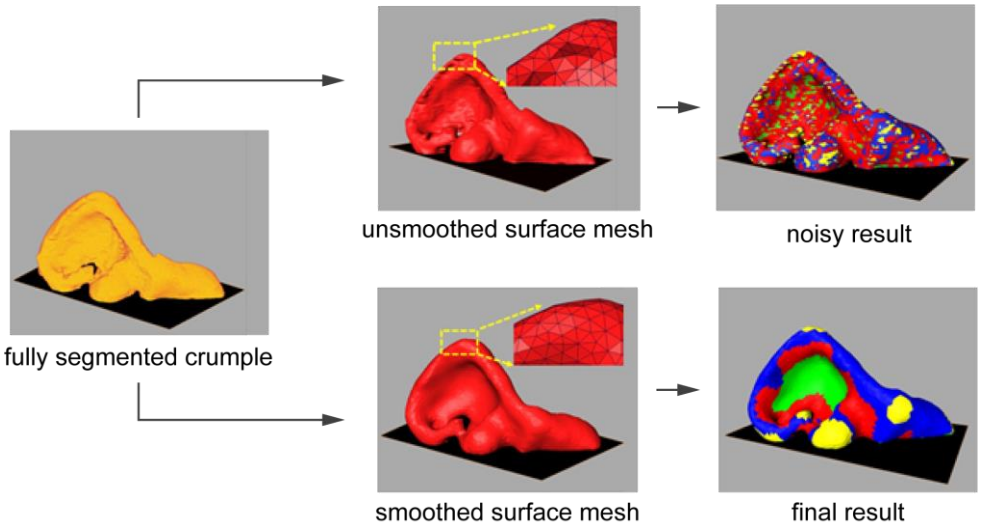

Figure S4. Flow chart of surface smoothing and the calculation of local curvature elements. top: A representative cluster crumple after segmentation, and the rough triangular mesh formed without smoothing. To the right is the unsmoothed mesh showing the noisy curvature element classification that results without smoothing. bottom: 3D triangular surface and 3D curvature element colormap after surface smoothing. The same smoothing parameters were applied to all crumples, as described in the Supplementary Methods.

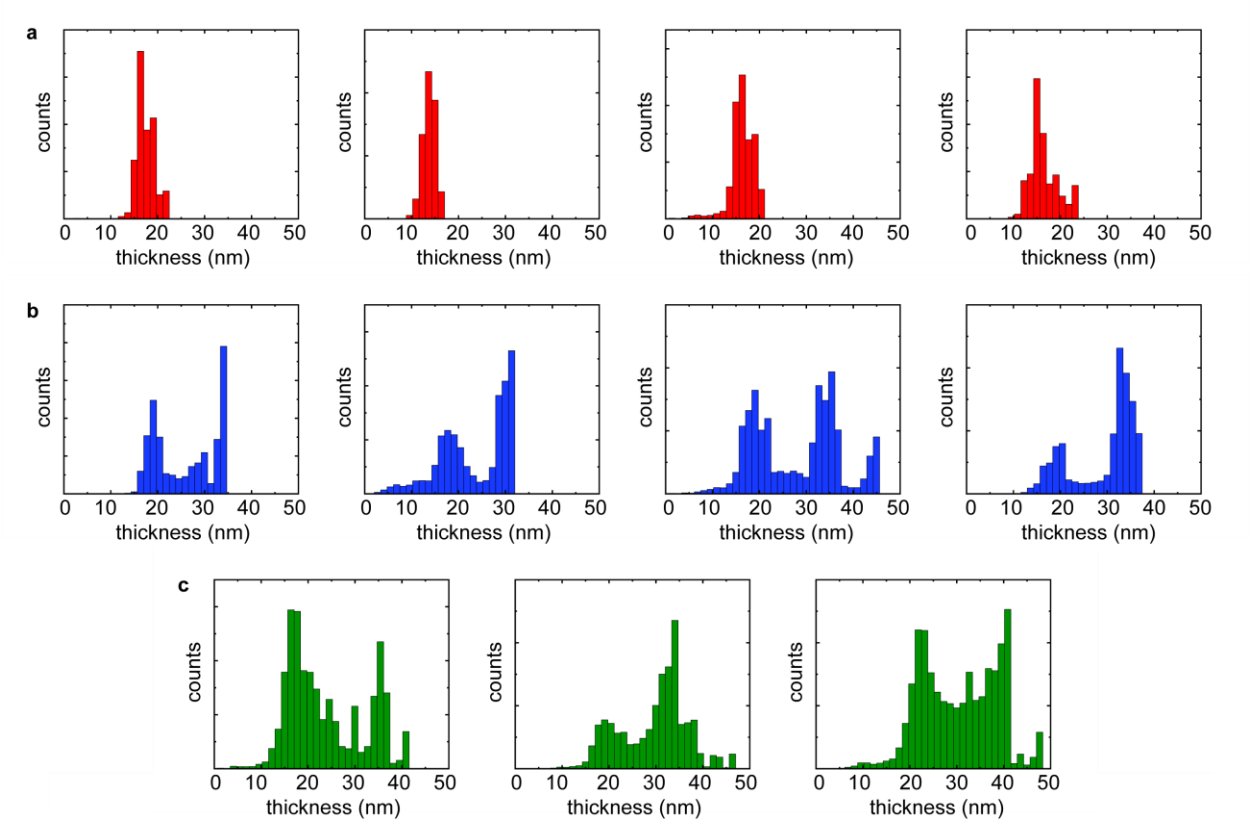

Figure S5. Complete thickness distributions of each of the 11 crumples analyzed. These distributions were summed by crumple type to produce Figure 3f–h in the main text. a) From left to right, thickness distributions of dome crumples 1–4. b) From left to right, thickness distributions of dimple crumples 1–4. c) From left to right, thickness distributions of cluster crumples 1–3.

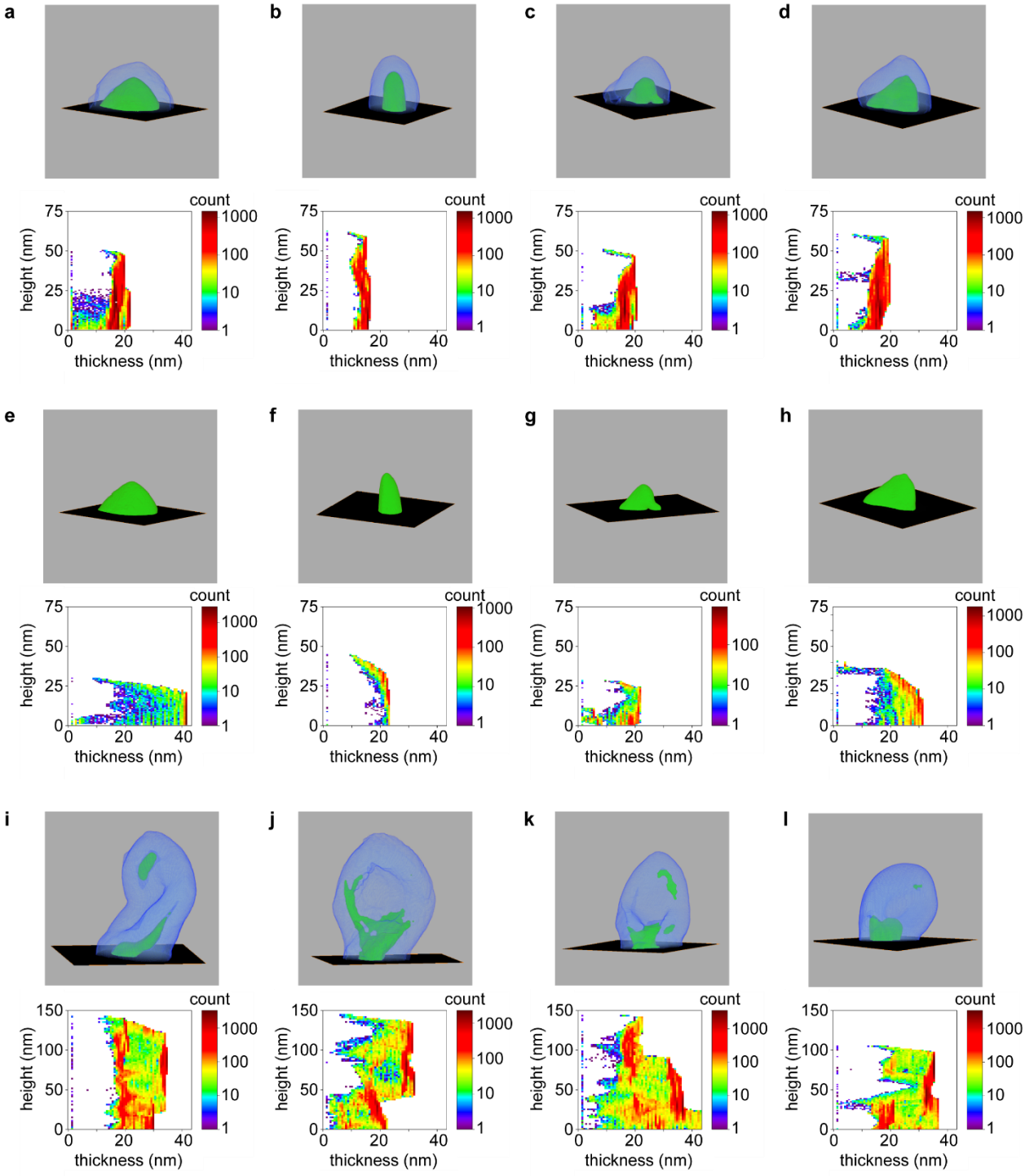

Figure S6. 3D visualization of crumples and corresponding thickness vs. height colormaps. a–d) top: dome crumples 1–4 and bottom: thickness vs. height maps, illustrating the approximately uniform thickness throughout the dome crumples. e–h) top: the voids of dome crumples 1–4 and bottom: the thickness vs. height maps of the voids. i–l) top: dimple crumples 1–4 and bottom: the thickness vs. height maps of dimple crumples 1–4. Note that all color bars are on a logarithmic scale.

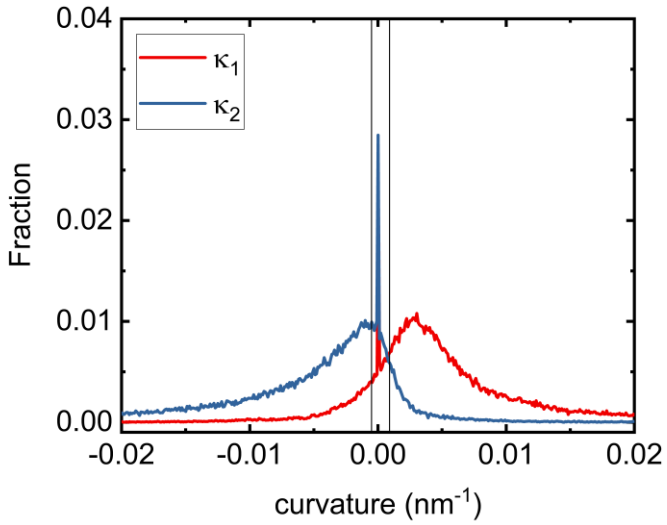

Figure S7. Example selection of the thresholds for κ_2 to distinguish the four curvature elements (Figure 2e and 2h in the main text). Thresholds were estimated on either side of the sharp peak near zero in the distribution of κ_2 values exhibited by all crumple types.

Tables S1–S4

Table S1: Size parameters of all analyzed crumples. Averages and ranges for various crumple types appear in the body of the main text. V: volume, A: surface area, A_{fp}: footprint area, m: mass, V_{void}: volume of the void, f_{void}: void volume fraction.

Crumple	$\boldsymbol{V}$ **(nm^3)**	$\boldsymbol{A}$ **(nm^2)**	$\boldsymbol{A/V}$ **(nm^{-1})**	$\boldsymbol{A_{\mathrm{fp}}}$ **(nm^2)**	$\boldsymbol{A/A_{\mathrm{fp}}}$	$\boldsymbol{m/A}$ **(μg/cm^2)**	$\boldsymbol{V_{\mathrm{void}}}$ **(nm^3)**	$\boldsymbol{f_{\mathrm{void}}}$
Dome 1	1.20×10^5	1.87×10^4	0.155	5.33×10^3	3.50	0.839	2.95×10^4	0.245
Dome 2	7.45×10^5	1.35×10^4	0.181	2.04×10^3	6.61	0.720	1.62×10^4	0.218
Dome 3	8.02×10^5	1.39×10^4	0.173	3.07×10^3	4.53	0.750	1.26×10^4	0.157
Dome 4	1.16×10^5	1.87×10^4	0.161	3.81×10^3	4.91	0.806	3.26×10^4	0.280
Dimple 1	4.97×10^5	5.09×10^4	0.102	5.15×10^3	9.88	1.27	2.32×10^4	0.047
Dimple 2	4.34×10^5	5.20×10^4	0.120	3.32×10^3	15.7	1.09	3.43×10^4	0.079
Dimple 3	5.49×10^5	5.51×10^4	0.100	5.87×10^3	9.39	1.30	2.81×10^4	0.051
Dimple 4	3.57×10^5	3.56×10^4	0.100	4.32×10^3	8.24	1.31	1.92×10^4	0.054
Cluster 1	1.57×10^6	1.78×10^5	0.114	3.02×10^4	5.89	1.14	4.70×10^5	0.30
Cluster 2	2.35×10^6	2.09×10^5	0.089	2.69×10^4	7.77	1.46	1.38×10^5	0.059
Cluster 3	2.46×10^6	2.19×10^5	0.089	3.72×10^4	5.89	1.46	9.80×10^4	0.040

Table S2: Fractions of different curvature elements for each crumple (as shown in Figure 2).

Crumple	% tip	% tube	% saddle	% valley	$\bar{G}$ (nm^{-1})	$\bar{H}$ (nm^{-1})
Dome 1	17.7	74.8	4.81	2.51	6.2×10^{-4}	4.6×10^{-3}
Dome 2	15.6	80.2	3.04	1.15	8.2×10^{-4}	6.9×10^{-3}
Dome 3	18.9	71.9	5.40	3.80	7.6×10^{-4}	7.9×10^{-3}
Dome 4	13.8	79.8	3.93	2.38	6.7×10^{-4}	5.8×10^{-3}
Dimple 1	24.8	40.6	14.6	20.1	3.4×10^{-4}	4.4×10^{-3}
Dimple 2	25.2	39.6	12.2	20.0	1.6×10^{-4}	7.7×10^{-3}
Dimple 3	23.2	41.9	16.0	19.0	2.5×10^{-4}	4.3×10^{-3}
Dimple 4	24.2	39.2	14.8	21.8	1.5×10^{-4}	1.0×10^{-2}
Cluster 1	8.43	34.6	33.0	23.9	1.8×10^{-4}	-4.5×10^{-3}
Cluster 2	9.7	35.2	32.3	22.8	1.9×10^{-4}	-2.4×10^{-3}
Cluster 3	10.6	36.1	32.0	21.3	2.3×10^{-4}	-2.2×10^{-3}

Table S3: Summary of 3D skeletonization parameters for each crumple type (as summarized in Figure 4d).

Crumple	# nodes	# branches	# points
Dome 1	59	59	894
Dome 2	68	67	942
Dome 3	24	26	610
Dome 4	63	62	1004
Dimple 1	112	111	1986
Dimple 2	234	236	3671
Dimple 3	57	64	1208
Dimple 4	67	67	1189
Cluster 1	691	702	11762
Cluster 2	681	684	11843
Cluster 3	584	587	10941

Table S4: Curvature thresholding value (κ_2) for different crumples shown in the main text. See Figure S7 for how these thresholds were chosen. A description of i and j appears in the Supplementary Methods.

Crumple	i **(nm^{-1})**	j **(nm^{-1})**
Dome 1	0.003	−0.004
Dome 2	0.001	−0.001
Dome 3	0.002	−0.003
Dome 4	0.0028	−0.003
Dimple 1	0.001	−0.001
Dimple 2	0.001	−0.001
Dimple 3	0.001	−0.0006
Dimple 4	0.0012	−0.001
Cluster 1	0.001	−0.0005
Cluster 2	0.0009	−0.0005
Cluster 3	0.0012	−0.0006

Captions for Movies S1–S2

Movie S1: 3D views of the full PA membrane reconstructed in IMOD and rendered in Amira. The crumples have a wide variety of morphologies but can be classified based on various shape parameters.

Movie S2: Slices and distributions showing the variation of local thickness throughout representative dome, dimple, and cluster crumples. Moving up through the sample, especially for the dimple crumple it can be seen that the thickest regions (bright yellow to white in color) appear when an internal void has been collapsed by two layers of the PA film coming into contact with one another. Scale bars: 50 nm.

Supplementary References

(1) Karan, S.; Jiang, Z.; Livingston, A. G. Sub–10 Nm Polyamide Nanofilms with Ultrafast Solvent Transport for Molecular Separation. *Science* **2015**, *348* (6241), 1347–1351.

(2) Kremer, J. R.; Mastronarde, D. N.; McIntosh, J. R. Computer Visualization of Three-Dimensional Image Data Using IMOD. *J. Struct. Biol.* **1996**, *116* (1), 71–76.

(3) Schindelin, J.; Arganda-Carreras, I.; Frise, E.; Kaynig, V.; Longair, M.; Pietzsch, T.; Preibisch, S.; Rueden, C.; Saalfeld, S.; Schmid, B.; Tinevez, J. Y.; White, D. J.; Hartenstein, V.; Eliceiri, K.; Tomancak, P.; Cardona, A. Fiji: An Open-Source Platform for Biological-Image Analysis. *Nat. Methods* **2012**, *9* (7), 676–682.

(4) Stalling, D.; Westerhoff, M.; Hege, H.-C. *Amira: A Highly Interactive System for Visual Data Analysis*; 2005.

(5) Dougherty, R.; Kunzelmann, K.-H. Computing Local Thickness of 3D Structures with ImageJ. *Microsc. Microanal.* **2007**, *13* (S02), 1678–1679.